INT. J. ELECTRONICS, 1989, VOL. 66, NO. 2, 227–245

Quantum modelling of charge distribution in single and multiple heterojunction modfets‡

SORIN VOINIGESCU†

A quantum model is derived and implemented for the detailed investigation of high-speed and high-frequency quantum devices. For the first time the electron wave-functions and depth profiles are computed for single- and multiple-quantum well MODFETs. The charge distribution in the channel(s) reveals multiple local maxima in agreement with experimental data. The influence of bias conditions and device parameters is studied at room- and liquid nitrogen temperatures. Finally, the limits of classical approaches using Fermi-Dirac statistics, or analytic formulations, are discussed. The latter is found to be conducive to a reduced spreading of the electron profile in the channel, with direct influence on the value of the gate capacitance.

1. Introduction

The last years have marked an ever-increasing interest in heterojunction devices as most suited applicants for very high speed logic (VHS) and monolithic-microwave (MM) integrated circuits. Two of the most versatile and promising heterostructure devices are the Heterojunction Bipolar Transistor (HBT) and the Modulation-Doped Field Effect Transistor (MODFET), the latter also known as the High Electron Mobility Transistor (HEMT) and the Two-Dimensional Electron Gas Transistor (TEGFET). Both devices require very accurate control of layer doping and layer thickness, as well as band geometry engineering. The basic material used in the fabrication of these devices is the AlGaAs/GaAs system (Morkoç *et al.* 1978). For room temperature operation (and especially for HBTs) the InP/InGaAs combination appears more promising due to higher band offsets and larger electron velocity.

The MODFET is by now a mature device with a variety of designs (Thorne *et al.* 1983), including complementary structures (Matsumoto *et al.* 1985), whose operation resembles in many respects the behaviour of MOS and MIS field-effect transistors. In this case, however, the channel electrons (or holes) are confined in a quasi-triangular or rectangular potential well to form a quantized two-dimensional gas (2-DEG or 2-DHG). Due to size-quantization the carriers occupy discrete energy levels in the narrow well. The number of excited (occupied) energy subbands and their energy values are extremely important for the correct evaluation of the two-dimensional carrier density and, eventually, for the derivation of the I-V curves and device parameters. It must be pointed out that, in MODFETs, quantizing effects and carrier transport appear (to a great extent) along mutually perpendicular

Received 1 October 1987; accepted 27 January 1988.

† Research & Development Center for Semiconductors and Electronic Components, Str. Erou Iancu Nicolae No. 32B, Sector 2, 72996, Bucharest, Rumania.

‡ This work was carried out while the author was with the Electronics Dept., Polytechnical Institute, Bucharest, Rumania.

0020 7217/89 $3.00 © 1989 Taylor & Francis Ltd.

Copyright © 2001. All Rights Reserved.

directions. This allows for the separate analysis of quantum and transport phenomena.

Most previous studies have focussed on the analytical or computer simulations of carrier transport. Quantum effects have been mainly analytically formulated (and included as such in computer simulations). Computer simulations addressing this topic are very few and refer to simple and idealized structures. Since device fabrication techniques have reached a high level of refinement, it becomes increasingly more apparent that the theoretical modelling of MODFETs also requires advanced sophistication that would facilitate large scale IC production.

Analytical and computer formulations of the electron-gas energies and sheet density in MODFETs (Schubert and Ploog 1985, Pierret 1985) have only dealt with the SH device neglecting tunnelling and carrier mass dependence on Al mole fraction and carrier energy (Vinter 1984, Stern and Das Sarma 1984, Yoshida 1986). An attempt has been made (Ravaioli and Ferry 1986) to apply a complete Monte Carlo investigation to an SH-MODFET. Although quite evolved, this approach has yet to include a more realistic model (i.e. other than the conventional analytical one) of the electron gas.

This paper presents a method for the accurate and very efficient simulation of the quantum effects in modulation-doped structures with arbitrary band geometry, which self-consistently solves the Schrödinger and Poisson equations. The approach applies equally well for n- and p-channel transistors and can be viewed as a starting point for the investigation of other quantum well devices such as Real-Space-Transfer Oscillators and the newly proposed quantum-base or quantum-emitter transistors (Chang *et al.* 1986).

The first section resumes the basics of quantum device physics and recasts the Schrödinger and Poisson equations in a form that includes energy-dependent mass effects, as well as impurity deionization via shallow and deep traps. Next, the mathematical formalism, based on a finite difference scheme, is developed. The final sections deal with results obtained through computer simulation of single and multiple heterojunction FET's, with an emphasis on electron wave-function profiles and quantum coupling in multiple channel devices.

2. Quantum physics of modulation-doped structures

In a conventional MODFET structure, the electron moves in an effective potential energy profile shown in Fig. 1 and described in eqn. (1).

$$V(z) = -qu(z) + E_0 - X_e(z) + V_{xc}(z) + V_{im}(z) \tag{1}$$

where $u(z)$ is the electrostatic potential, $X_e(z)$ is the position-dependent electron affinity, $V_{xc}(z)$ is the local exchange correlation potential energy and E_0 is the vacuum level potential energy (usually set at 0 eV).

In the case of an abrupt $Al_xGa_{1-x}As$/GaAs heterojunction, expressions for the image potential energy $V_{im}(z)$ and the local exchange correlation potential are available in the literature (Stern and Das Sarma 1984).

The wave function $\psi_i(z)$ of an electron in subband i is given by a Schrödinger equation of the BenDaniel–Duke form in which $V(z)$ is derived from eqn. (1) (Stern and Das Sarma, 1984, Vinter 1984).

$$-\hbar^2/2\; d/dz[1/m_e(z)\; d\psi_i(z)/dz] + V(z)\psi_i(z) = E_i\psi_i(z) \tag{2}$$

Copyright © 2001. All Rights Reserved.

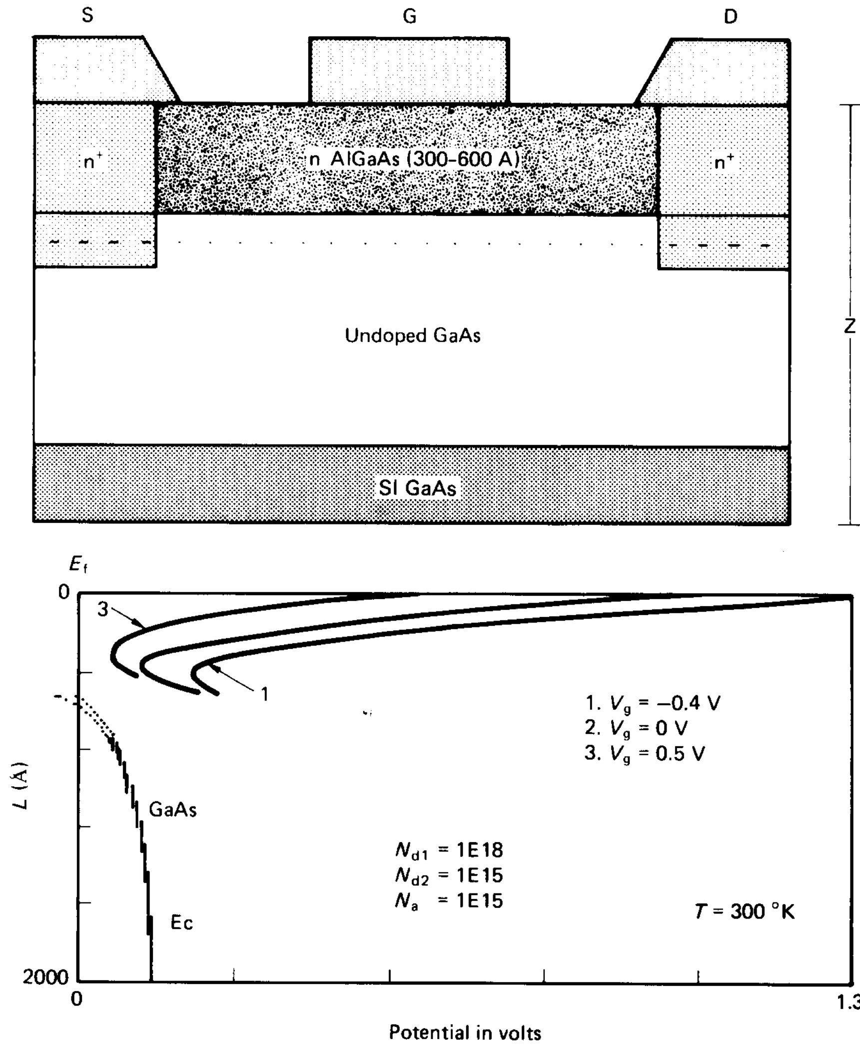

Figure 1. Conduction band outlines at various bias voltages in a conventional SH-MODFET.

and which must be solved in conjunction with Poisson's equation for the electrostatic potential

$$d/dz[K_0\, K(z)\; du(z)/dz] = q \sum_{i=0} N_i\, |\psi_i(z)|^2 - R_0(z) \tag{3}$$

where

$$N_i = m_{\mathrm{ch}}(E_i - V(z))K_{\mathrm{B}}\, T/(\pi\hbar^2) \ln\, [1 + \exp\, ((E_{\mathrm{F}} - E_{\mathrm{i}})/(K_{\mathrm{B}}\, T))] \tag{4}$$

is the position dependent 2-DEG density per electron energy and m_{ch} describes the energy-dependent carrier mass in the channel;

$$R_0(z) = q[N_{\mathrm{D}}^{+}(z) - N_{\mathrm{A}}(z) - n_{\mathrm{B}}(z)] \tag{5}$$

Copyright © 2001. All Rights Reserved.

represents the three-dimensional charge density and

$$n_B(z) = 2(\pi)^{-1/2} N_c(z) F_{1/2}([E_{Fn}(z) - E_c(z)]/(K_B T)) \tag{6}$$

is the three-dimensional free electron bulk charge. The ionized donor concentration in AlGaAs can be computed from Lee *et al.* 1983, Ponse *et al.* 1985:

$$N_D^+(z) = sN_D(z)/(1 + 2\exp[-(E_C - E_{Fn} - E_{Dsh})/(K_B T)]) + (1 - s)N_D(z)/(1 + 2\exp[-(E_C - E_{Fn} - E_{Dd})/(K_b T)]) \tag{7}$$

in which E_{Dsh} (40–50 meV) and E_{Dd} (0·4–0·6 eV) are the energy levels of the shallow and deep traps relative to the bottom of the conduction band, respectively, and s describes the proportion of shallow and deep traps in the overall impurity concentration.

The average electron gas sheet concentration in the quantum well is given by:

$$n_s = \sum_{i=0} \int_{Z_{int}}^{L} N_i(z) |\psi_i(z)|^2 \, dz \tag{8}$$

(Z_{int} and L are the positions of the heterojunction and substrate, respectively).

It should be underlined that a strong coupling exists between the Schrödinger and Poisson equations. First, the right-hand side of eqn. (3) depends on the wave functions ψ_i through N_i. Also, the wave functions are linked to the potential profile $u(z)$ due to the presence of $V(z)$ (actually the bottom of the conduction band) in the Schrödinger equation. The self-consistency is further enhanced if the energy-dependent mass replaces the effective mass model (as is the case of this paper).

The expressions presented above can be applied to solve the semiconductor equations at equilibrium in the z-direction, defined as the direction perpendicular to the interfaces. Since the size quantization acts only along this axis, and as the material parameters in eqns. (2) and (3) (m and K) are dependent on z alone, a two-dimensional analysis (along z and y axes) can be performed by solving the z-axis Schrödinger equation at each y location (to obtain the eigenvalues $E_i(y)$ and wave function surfaces $\psi_i(y, z)$ and the y-z Poisson equation with a conventional two-dimensional solver.

Because the two-dimensional analysis is a repetitive replica of the one-dimensional case, a simplified one-dimensional procedure will be considered further which enables a thorough investigation of the quantum-mechanical effects in a single- and multiple-quantum-well MODFETs. The latter have been given little attention in the literature and it is mainly the z-direction quantum modelling that deviates from the single heterojunction device.

3. Finite difference scheme

To simplify the computer simulation procedure and to avoid overflow and/or underflow, all equations have been normalized. The normalizing factors are listed in Table 1. They are similar to those usually employed in classical semiconductor simulations. The only difference rests with the device coordinates and carrier-density normalizing factors, which have been modified to better scale the submicron dimensions of MODFET structures and to recast the Schrödinger equation in a simple format.

The formulae describing the material parameters of $Al_xGa_{1-x}As$ have been taken from Kawai *et al.* 1984 and updated where necessary (Heiblum *et al.* 1985, Weiler and Ayasli 1984).

Copyright © 2001. All Rights Reserved.

Parameter to normalize	Normalization factor	(expression and value for GaAs)
x, y, z	$L_D = \hbar/(2m_e K_B T)^{1/2}$	47·1 Å
u	$V_t = K_B T/q$	0·02584 V
E, E_i	$E_t = K_B T$	4·14E-21 J
ψ_i	$\psi_t = 1/L_D^{1/2}$	1457·1 $\text{cm}^{-1/2}$
$N_{D,A}, n_B$	$n_t = K_0 K V_t/(qL_D^2)$	8·412E17 cm^{-3}
N_s, n_s, N_i	$n_{st} = n_t L_D$	3·962E11 cm^{-2}
D_p, D_n	D_t	1 cm^2/s
t	$t_t = L_D^2/D_t$	2·2184RE-13 s
J_p, J_n, J	$J_t = -qD_t n_t/L_D$	2·86E6 A/cm^2
R, G, U	$U_t = D_t n_t/L_D^2$	3·79E30 $\text{s}^{-1}\,\text{cm}^{-3}$
μ_p, μ_n	$\mu_t = D_t/V_t$	38·699 cm^2/Vs
v_p, v_n	$v_t = D_t/L_D$	2·123E6 cm/s
α_p, α_n	$\alpha_t = 1/L_D$	2·123E6 cm^{-1}
Area	$A_t = L_D^2$	2·2184E-13 cm^2
Impedance	$Z_t = V_t/(qD_t n_t L_D)$	4·07E6 Ω

Table 1. Normalization factors used in computer simulation.

$$E_C = 0{\cdot}65[1{\cdot}247x + 1{\cdot}147(x - 0.45)^2]$$

$$E_V = 0{\cdot}35[1{\cdot}247x + 1{\cdot}147(x - 0{\cdot}45)^2]$$

$$N_c = 2{\cdot}508\text{E}19(T/300)^{3/2}(0{\cdot}067 + 0{\cdot}083x)^{3/2}\,(\text{cm}^{-3})$$

$$N_h = 2{\cdot}508\text{E}19(T/300)^{3/2}[(0{\cdot}068 + 0{\cdot}192x)^{3/2} + (0{\cdot}5)^{3/2}]\,(\text{cm}^{-3})$$

$$\phi_B = 0{\cdot}85 + 0{\cdot}62x$$

$$K = 12{\cdot}9 - 2{\cdot}9x$$

$$m_{hh} = (0{\cdot}48 + 0{\cdot}31x)m_0$$

$$m_e = m_e^{\text{GaAs}} + 0{\cdot}083xm_0$$

For GaAs the following expressions have been employed.

$$m_e(E) = (0{\cdot}0665 + 0{\cdot}0436E + 0{\cdot}0236E^2 - 0{\cdot}147E^3)m_0$$

$$E_g(T) = 1{\cdot}519 - 5{\cdot}405E - 4T^2/(204 + T)$$

(all energies are in eV).

Throughout this section, the parameters dependent on the Al mole fraction x, will be normalized to those of GaAs and noted with the '*' superscript (for example, $m_e^*(z) = m_e(z)/m_e^{\text{GaAs}}$).

With these observations, the initial equations are recast in normalized form (the symbols of the original variables have been retained).

$$V = u + E_0 - X_e + V_{xc} + V_{im} \tag{1a}$$

$$\nabla(1/m_e^* \nabla\psi_i) + (E - V)\psi_i = 0 \tag{2a}$$

$$\nabla(K^*\nabla u) = \sum_{i=0} N_i |\psi_i|^2 - R_0 \tag{3a}$$

Applying the finite difference scheme in the one-dimensional case, the following systems of discrete linear equations are obtained.

Copyright © 2001. All Rights Reserved.

$$b_{j-1}\psi_{j-1} + a_j\psi_j + b_j\psi_{j+1} = 0 \tag{9}$$

$$b_{j-1}u_{j-1} + a_j u_j + b_j u_{j+1} = (h_j + h_{j-1})(n_{CHj} - R_{0j}) \tag{10}$$

where $j = 1, \ldots, N - 1$; ($N + 1$ is the number of meshpoints),

$h_j = z_{j+1} - z_j$ (local mesh-step),

$a_j = (E - V_j)(h_j + h_{j-1}) - (1/m_j^* - 1/m_{j+1}^*)/h_j - (1/m_j^* + 1/m_{j-1}^*)/h_{j-1}$,

$b_j = (1/m_j^* + 1/m_{j+1}^*)/h_h$ (for eqn. (9)) and

$a_j = -[(K_j^* + K_{j+1}^*)/h_j + (K_j^* + K_{j-1}^*)/h_{j-1}]$,

$b_j = (K_j^* + K_{j+1}^*)/h_j$ (for eqn. (10))

ψ_j and u_j are sampled values of ψ and u, respectively, at meshpoint j, while $n_{CHj} - R_{0j}$ is the sampled right-hand side of eqn. (3).

Solving eqn. (10) poses no problems as it has been thoroughly treated in the literature. Equation (9) represents a homogeneous system of $N - 1$ equations with $N + 1$ unknowns. Two more equations are added by imposing the continuity of the wave-function and its derivative at the boundaries ($z_0 = 0$ and $z_N = L$) (Messiah 1970). The matrix of this system is tridiagonal and symmetric and its determinant (D_N) must be nil so that non-zero solutions can be found.

$$D_N = \begin{vmatrix} a_0 & b_0 & 0 & 0 & 0 & 0 & \cdots & 0 & 0 & 0 & 0 \\ b_0 & a_1 & b_1 & 0 & 0 & 0 & \cdots & 0 & 0 & 0 & 0 \\ 0 & b_1 & a_2 & b_2 & 0 & 0 & \cdots & 0 & 0 & 0 & 0 \\ 0 & 0 & b_2 & a_3 & b_3 & 0 & \cdots & 0 & 0 & 0 & 0 \\ \hline 0 & 0 & 0 & 0 & 0 & 0 & \cdots & 0 & b_{N-2} & a_{N-1} & b_{n-1} \\ 0 & 0 & 0 & 0 & 0 & 0 & \cdots & 0 & 0 & b_{N-1} & a_N \end{vmatrix} = 0 \tag{11}$$

where

$$a_0 = -(1 + h_0 B_0)b_0; \quad a_N = -(1 + h_{N-1}B_N)b_{N-1}$$

and

$$B_0 = [m_0^*(V_0 - E)]^{1/2}; \quad B_N = [m_N^*(V_N - E)]^{1/2}$$

D_N can be computed using the recursive scheme

$$D_{-1} = 1; \quad D_0 = a_0; \quad D_k = a_k D_{k-1} - b_{k-1}^2 D_{k-2} \tag{12}$$

Relation (11) represents a nonlinear equation in E whose zeros are the energy eigenvalues E_i. To solve it, a Newton-type algorithm has been employed. The electron wave-function is fully determined by imposing the normalizing condition

$$\sum_{j=0}^{N} |\psi_j|^2 h_j = 1 \tag{13}$$

Copyright © 2001. All Rights Reserved.

A similar treatment can be applied to the discretized Poisson eqn. (10) to obtain a nonhomogeneous system of linear equations in which the unknowns are the correction potentials $\Delta u_j^{k+1} = u_j^{k+1} - u_j^k$ (superscripts refer to iteration number).

$$b_{j-1}\Delta u_{j-1} + A_j \Delta u_j + b_j \Delta u_{j+1} = D_j \tag{10a}$$

$$A_j = a_j - [N_D^+/(1 + 0{\cdot}5 \exp(+E_{Cj} - E_{Fj} - E_{Dj})) + dn_{Bj}/du_j](h_j + h_{j-1})$$

$$D_j = (h_j + h_{j-1})(n_{CHj} - R_{0j}) - b_{j-1}u_{j-1} - a_j u_j - b_j u_{j+1}$$

$$j = 1, 2, \ldots, N-1.$$

A_j contains information regarding the derivatives of the free electron bulk charge n_B and of the ionized impurity profile in the case of shallow traps (deep traps are included in a similar manner). This informations speeds up convergence. Also, both A_j and D_j express the self-consistency with the Schrödinger equation due to the presence of $E - V_j$ in a_j and n_{CHj} in D_j, respectively.

The potential is determined by solving eqn. (10a) with the proper boundary conditions:

$$E_0 = X_e^{GaAs} + E_g^{GaAs}/2$$

$$u_0 = V_G - \phi_B + E_g(0)/2$$

$$\Delta u_0 = 0; \quad du_N/dz = 0$$

Because in the normal range of gate bias the gate currents are very low (Ponse, Masselink and Morkoç 1985), the quasi-Fermi level E_F is assumed to be constant throughout the simulation region. This is a minor and habitual approximation (Vinter 1984, Stern and Das Sarma 1984) which prevents the inclusion of the additional current balance equation.

Based on the above algorithms, the simulation starts by iteratively solving the Poisson equation until a reasonable potential change between two successive iterations is achieved (usually below 1 mV). Quantum effects are neglected at this stage and Fermi statistics are assumed. We use a nonuniform discretization mesh and an analytic initial solution. The computational process continues with the alternate iterative solving of the Schrödinger and Poisson equations until the desired precision is gained. After each Poisson iteration, the electric potential u_j is updated using a damping coefficient to improve convergence: $u_j^{k+1} = u_j^k + r\Delta u_j^{k+1}$. The damping coefficient depends on device temperature and takes values between 0·1 and 1 (at low temperatures small r values are required). The Schrödinger equation is solved with floating left- and right-hand boundaries (in a device zone surrounding the heterointerface, that expands as the two-dimensional electron-gas energies become larger). First, the eigen-energies are obtained in a Newton-loop from eqn. (11). The electron wave functions and the corresponding subband electron populations are then computed throughout the well region. Based on the physical properties of the solution (Messiah 1970), the WKB approximation is used to derive wave function and electron profiles in the barrier layers, away from the well. This procedure severely shrinks computation time in the Schrödinger iteration and allows for the correct evaluation of tunnelling effects.

More investigation of the wave-function boundary conditions' influence on simulation results must be performed since different sets of boundary conditions

Copyright © 2001. All Rights Reserved.

have been employed by other authors. For instance, Yoshida (1986) assumes vanishing wave-functions at fixed gate and substrate boundaries, while Laux and Stern (1986) consider, more in line with present work and physical consistency, that the wave functions must be conserved at these boundaries. The next paragraph elaborates on this aspect.

The most time-consuming part of the computational scheme is the Newton-loop, which solves the transcendental eigenvalue eqn. (11). The problem lies with separation of the intervals containing each eigenvalue and it becomes extremely complicated in multiple channel devices. A study of the solution behaviour has indicated that, in all cases, the position of the energy eigenvalues, relative to the minimum of the conduction band energy in the well, changes only slightly from one iteration to the other, while the whole frame of the energy profile of the quantum well shifts upwards or downwards. Consequently, the eigenvalue intervals can be fast separated using information from the previous iteration concerning energy eigenvalues.

The computation time with this algorithm is no more than twice that required for the analysis of unipolar heterojunction devices under similar conditions (comparable mesh, Gauss solver for linear systems, etc.) while the store-core remains roughly the same even with the introduction of a third equation for carrier continuity. As a conseqence, this algorithm can be efficiently extended for the two-dimensional quantum simulation of quantum well devices. The one-dimensional program has been implemented in Turbo-Pascal and a shortened pseudo-code version of the algorithm is listed below.

```
InitialProblemDefinition
WHILE max(Δu_j) > 1 meV DO
BEGIN
  EvaluatePoissonCoefficients
  SolvePoissonEquation
  u_j := u_j + r_1 Δu_j
END
1:WHILE max(Δu_j) > 0·01 meV DO
  BEGIN

    EvaluateSchrödingerCoefficients
    SeparateEigenvalueIntervals
    DetermineE_iNumber:NE
    FOR i := 1 TO NE DO
    BEGIN
      NewtonLoopForE_i
      Compute ψ_{i,j}, N_{i,j}, |ψ_j|^2
    END
    n_CHj := Σ_{i=1}^{NE} N_{i,j} |ψ_{i,j}|^2
    EvaluatePoissonCoefficients
    SolvePoissonEquation
    u := u_j + r_2 Δu_j
  END

IncrementGateVoltage
GOTO 1.
```

Copyright © 2001. All Rights Reserved.

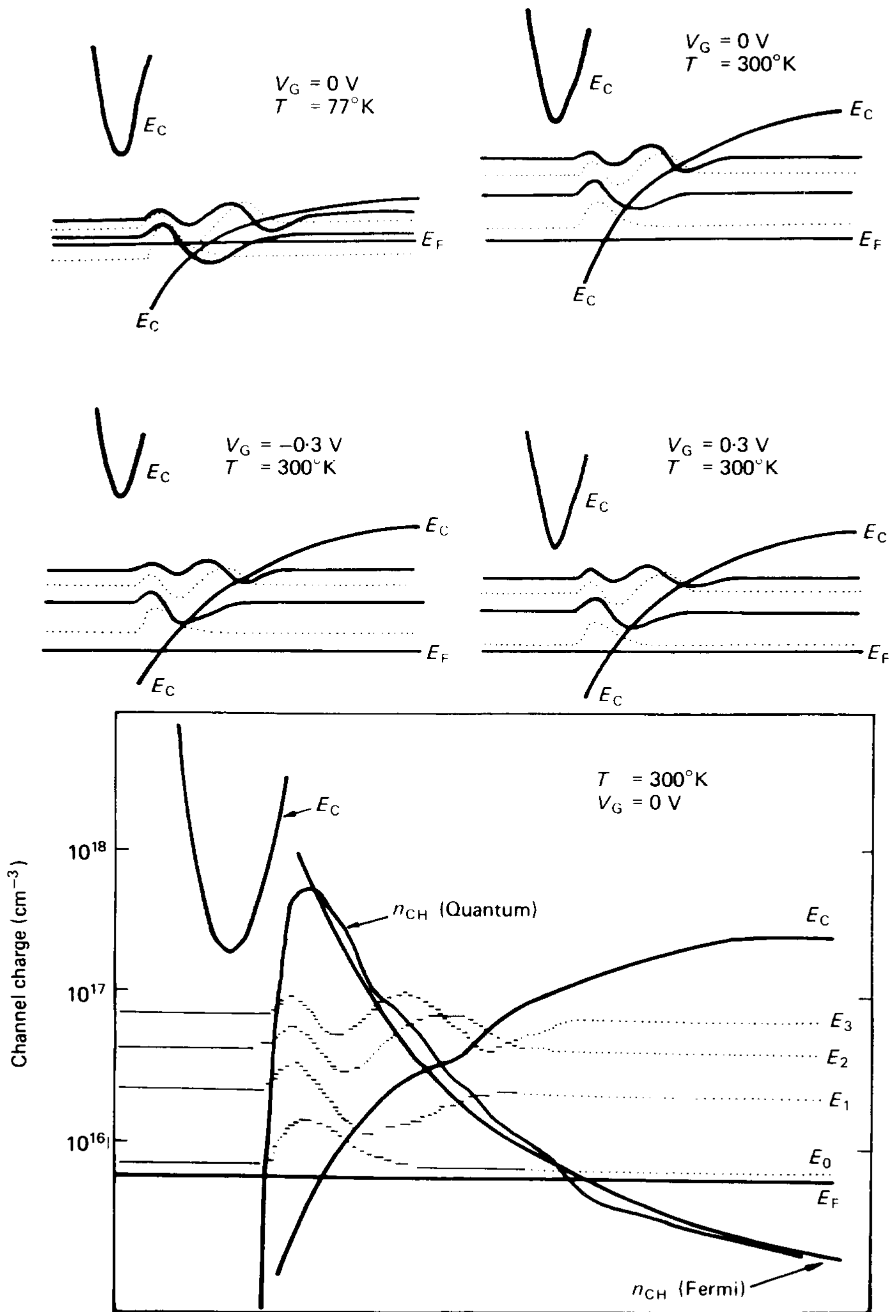

Figure 2. Electron wave function and depth profiles in an SH-MODFET at 300 °K and 77 °K for various gate voltages. The device has 0·3 Al mole fraction and the thickness of the AlGaAs region ($N_d = 10^{18}\,cm^{-3}$) is 500 Å (a normally-ON device) including an undoped ($N_d = 10^{15}\,cm^{-3}$) 50 Å spacer layer. The GaAs channel has a thickness of 1500 Å and an unintentional doping of $10^{15}\,cm^{-3}$ (p-type). Electron charge profiles obtained through quantum and Fermi-Dirac simulations are compared in the bottom graph.

Copyright © 2001. All Rights Reserved.

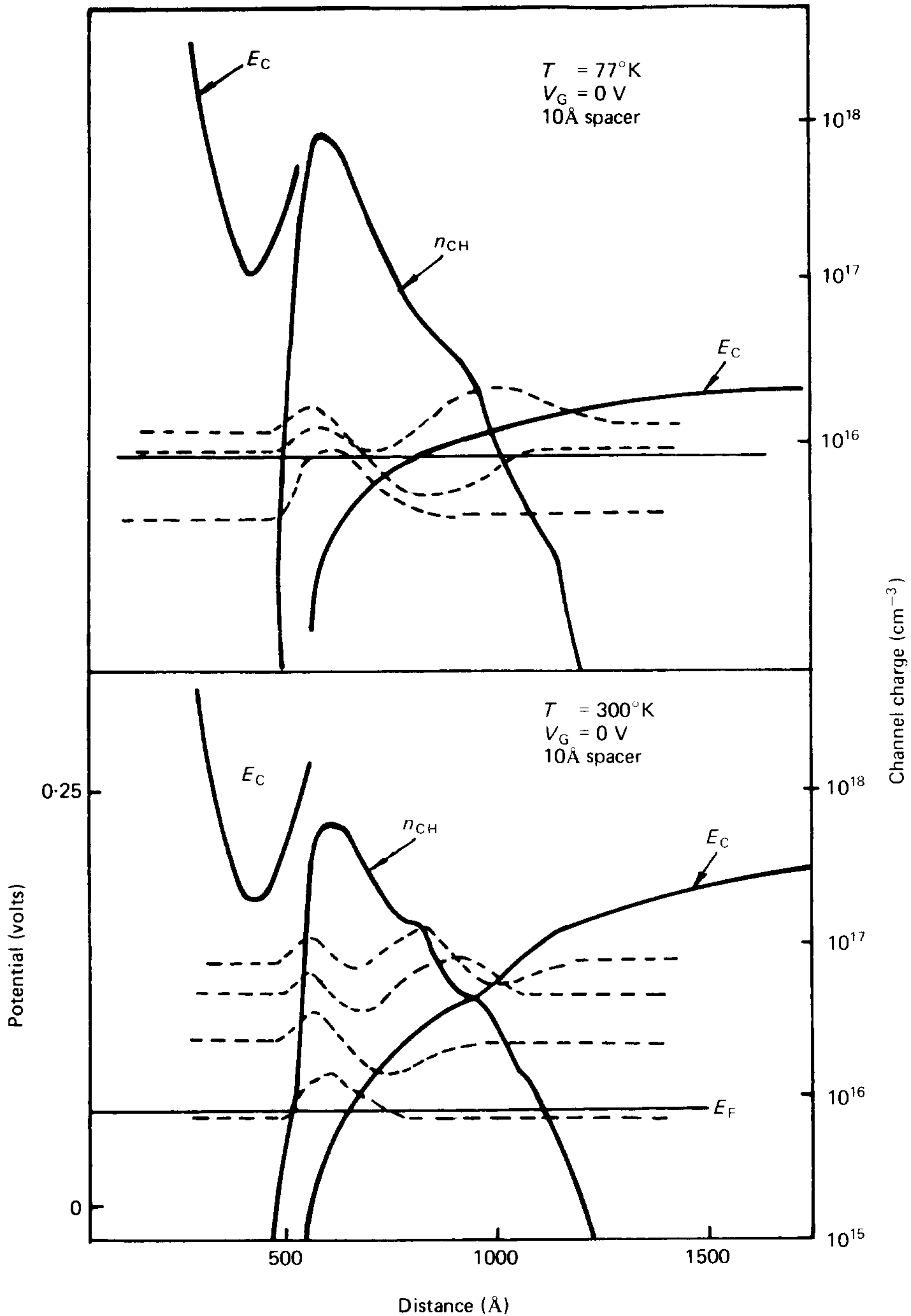

Figure 3. 2-DEG profiles computed with the energy-dependent-mass model in an SH-MODFET identical to the one in Figure 2, except for the 10 Å undoped spacer. The eigen-energies, relative to the minimum of the conduction band are listed below.

77 °K	$E_0 = 0{\cdot}0618\,\mathrm{eV}$;	$Ns_0 = 8.428\ 10^{11}\,\mathrm{cm}^{-2}$;
	$E_1 = 0{\cdot}0955\,\mathrm{eV}$;	$Ns_1 = 0{\cdot}808\ 10^{11}\,\mathrm{cm}^{-2}$;
	$E_2 = 0{\cdot}1079\,\mathrm{eV}$;	$Ns_2 = 0{\cdot}151\ 10^{11}\,\mathrm{cm}^{-2}$;
300 °K	$E_0 = 0{\cdot}0624\,\mathrm{eV}$;	$Ns_0 = 5{\cdot}917\ 10^{11}\,\mathrm{cm}^{-2}$;
	$E_1 = 0{\cdot}1070\,\mathrm{eV}$;	$Ns_1 = 1{\cdot}497\ 10^{11}\,\mathrm{cm}^{-2}$;
	$E_2 = 0{\cdot}1312\,\mathrm{eV}$;	$Ns_2 = 0{\cdot}632\ 10^{11}\,\mathrm{cm}^{-2}$;
	$E_3 = 0{\cdot}1466\,\mathrm{eV}$;	$Ns_3 = 0{\cdot}361\ 10^{11}\,\mathrm{cm}^{-2}$;
	$E_4 = 0{\cdot}1588\,\mathrm{eV}$;	$Ns_4 = 0{\cdot}231\ 10^{11}\,\mathrm{cm}^{-2}$.

Copyright © 2001. All Rights Reserved.

Most of the performed calculations have been carried out with a non-uniform mesh of 150 to 400 points.

4. Results and discussions

4.1. *Behaviour of single-heterojunction FETs*

$Al_xGa_{1-x}As$ n-channel SH-MODFET structures have been simulated. To keep in line with more recent experimental results, 65% rather than 85% of the bandgap difference is assumed to lie in the conduction band at the AlGaAs/GaAs interface. Lack of reliable material data has prevented the study of devices in other material systems.

Figures 2 and 3 present one-dimensional computer-analysis electron wave-function and charge profiles in an SH-MODFET, for various gate voltages, at 300 °K and 77 °K. Before interpreting the results, we refer to the literature for an evaluation of their reliability by comparison with experimental and theoretical data (Schubert and Ploog 1985, Hikosaka *et al.* 1986, Pospieszalski *et al.* 1986, Takakuwa *et al.* 1986).

Since actual subband energies might vary from case to case in theoretical calculations (depending on the choice of potential energy reference), their mutual spacing or separation from the channel imref, which is independent of the energy reference, will be considered further. Comparison with other self-consistent simulations is slightly hampered by the lack of real-device results. Most of the calculations performed in literature concern idealized structures, particularly the AlGaAs/GaAs interface, and are not related to design-oriented parameters, such as gate voltage and donor doping (Stern and Das Sarma 1984). However, the variation of subband spacings as a function of the 2-DEG concentration is an intrinsic characteristic of an AlGaAs/GaAs heterojunction (linked to the band offset) and does not directly relate to gate voltage and donor doping in the AlGaAs barrier. (Actually, it is the 2-DEG concentration that depends on bias and ionized donors.) If this variation is compared to that of Stern and Das Sarma, computed in the effective mass approximation, agreement within 1% is achieved both at 77 °K and 300 °K. Also, despite the fact that the present work systematically predicts somewhat lower subband spacing (more in line with experimental data), our results on the device simulated by Yoshida (1986) with 85% of the bandgap offset residing in the conduction-band, give the same carrier distribution among the energy subbands. The only difference stems from the different carrier profile along the z-axis. One cause might rest with the choice of fixed-boundary conditions for the Schrödinger equation which could lead to over-elongated wave-functions, smoothing-out the electron profile. Another is related to the 0-volt substrate boundary condition in the Poisson equation that raises the level of the conduction band in GaAs and slightly increases subband spacing and the number of higher order eigenvalues.

Experimental data refer mostly to the overall carrier density in the channel. In the case of an SH-MODFET with a 490 Å, $1.5 \times 10^{18}\,cm^{-3}$ doped layer and 10 Å spacer (Takakuwa *et al.* 1986), the measured concentration, both at 77 °K and 300 °K, is $1{\cdot}2 \times 10^{12}\,cm^{-2}$. With 0·3 V gate bias at liquid nitrogen temperatures and 0·5 V at room temperature, the computations indicate $1{\cdot}18 \times 10^{12}$ and $1{\cdot}21 \times 10^{12}\,cm^{-2}$, respectively.

By examination of Figs. 2 and 3 and Table 2, it is noticed that, although the overall sheet charge is roughly the same, only 64% of the electron population

Copyright © 2001. All Rights Reserved.

T (°K)	$E_1 - E_0$ (meV)	$E_2 - E_1$ (meV)	N_0	N_1	N_2	N_3	N_s
			($10^{11}\,cm^{-2}$)				
1) 300	38·45	22·39	4·15	1·17	0·516	0·285	6·8
1) 77	26·47	13·31	6·6	0·92	0·153	0·057	7·7
2) 77	34·98	13·43	9·1	0·99	0·165	0·057	10·4
3) 77	25·84	—	4·875	0·435	—	—	5·31
4) 77	25·84	—	4·865	0·434	—	—	5·3
4) 5) 77	26·2	—	—	—	—	—	5·1
6) 77	97·91	—	13·41	1·03E-3	—	—	13·41
6) 300	99·39	—	10·96	0·533	—	—	11·5
7) 300	99·23	—	11·59	0·5975	—	—	12·17
8) 300	99·68	—	9·955	0·4417	—	—	10·397
9) 300	100·57	—	8·416	0·3196	—	—	8·735

1) SH-MODFET: $N_{D1} = 10^{18}\,cm^{-3}$; $N_{D2} = 10^{15}\,cm^{-3}$; $N_A = 10^{15}\,cm^{-3}$; $Z_{int} = 500$ Å; 50 Å spacer; $V_G = 0$ V.
2) Same as 1) but no spacer.
3) Same as 1) with 100 Å spacer.
4) Same as 3) but $N_A = 10^{14}\,cm^{-3}$.
5) Stern and Das Sarma 1984.
6) DH-MODFET: $N_{D1} = 10^{18}\,cm^{-3}$; $N_{Du} = 10^{15}\,cm^{-3}$; $N_A = 10^{14}\,cm^{-3}$; $N_{D3} = 5\ 10^{17}\,cm,^{-3}$; $Z_{int} = 500$ Å; 50 Å spacers; 100 Å channel; $V_G = 0$ V.
7) Same as 5) but $V_G = 0{\cdot}3$ V.
8) Same as 5) but $V_G = -0{\cdot}3$ V:
9) Same as 5) but $V_G = -0{\cdot}6$ V.

To facilitate comparison with other theoretical works, all simulated results are obtained within the effective mass approximation.

Table 2. Subband energies and sheet charge concentrations in MODFETs.

occupies the lowest energy level at 300 °K, as compared to 83% at 77 °K. Also, for the device in Fig. 2, at 300 °K and zero gate voltage, all subband energies are located above the channel imref (even at a positive gate bias of 0·7 V the lowest subband is slightly above the Fermi level). The higher electron energies contribute to the poor mobility values at this temperature. At 77 °K the first subband is well below the channel imref causing more than 80% of the carriers to travel at low energy levels and higher mobilities. This situation is mainly due to the large difference in the degree of AlGaAs impurity ionization at low and high temperatures, respectively, which greatly alters the conduction band profile in the channel and bulk GaAs. Energy spacing is larger at 300 °K because of the larger value of the conduction band energy at the substrate boundary. This also influences the degree of electron wave-function spreading, which tends to be slightly more pronounced

Copyright © 2001. All Rights Reserved.

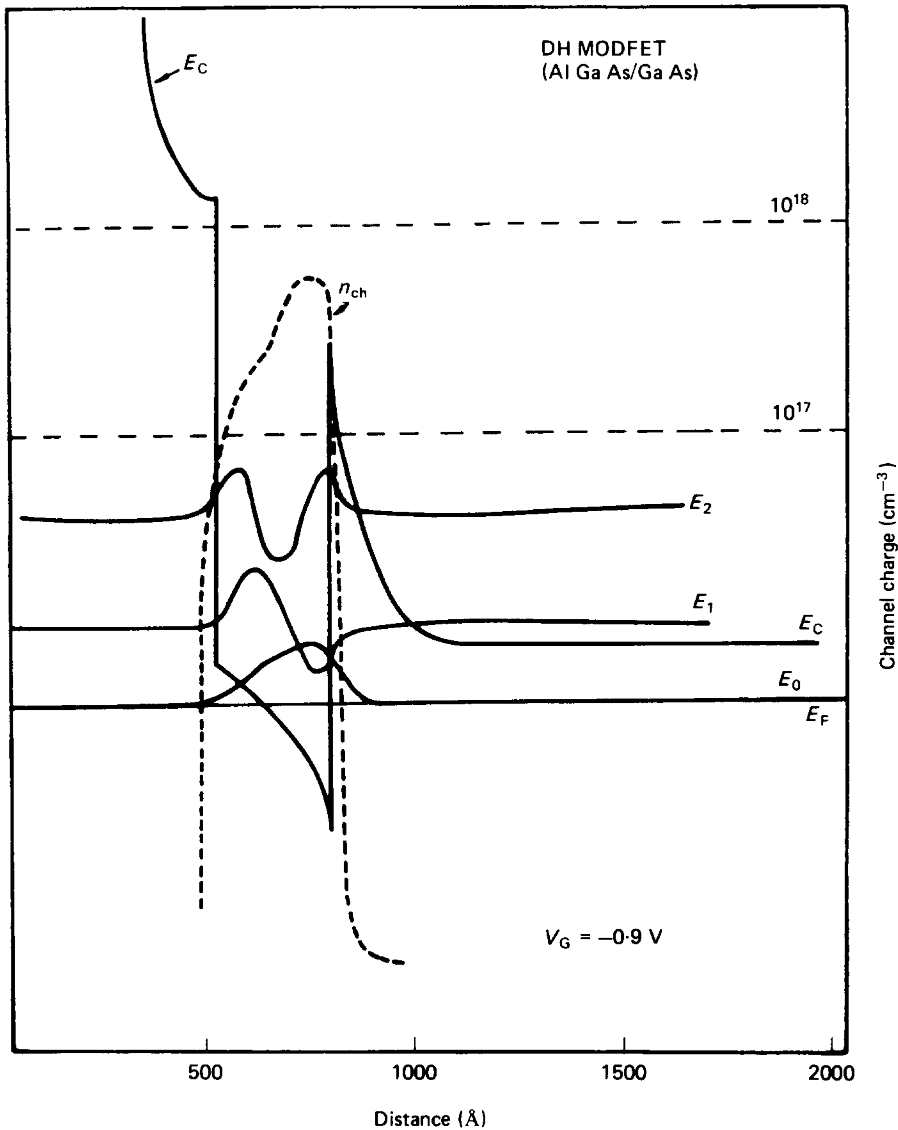

Figure 4. Electron profiles in a reverse biased DH-MODFET at room temperature. The device is identical to the one in Table 2, except for the 0·24 Al mole fraction and the 200 Å-well. The eigen-energies, relative to the minimum of the conduction band, are listed below. Energy-dependent mass was considered in the channel.

$$E_0 = 0{\cdot}0537\,\text{eV};\quad Ns_0 = 3{\cdot}642\ 10^{11}\,\text{cm}^{-2};$$
$$E_1 = 0{\cdot}0925\,\text{eV};\quad Ns_1 = 0.981\ 10^{11}\,\text{cm}^{-2};$$
$$E_2 = 0{\cdot}1415\,\text{eV};\quad Ns_2 = 0{\cdot}161\ 10^{11}\,\text{cm}^{-2}.$$

with higher 77 °K subbands and is related to increased tunnelling in bulk GaAs as the right-hand barrier height lowers. A similar explanation stands for the wave-function spreading as the gate voltage shifts to lower and negative values. The spreading mainly affects the rightmost lobe of the electron wave-function associated to each energy eigenvalue. This lobe presents larger heights and widths than those to its left, suggesting that most of the subband population is concentrated away

Copyright © 2001. All Rights Reserved.

from the heterointerface (Fig. 3). Hence the relatively good estimations obtained with Schubert and Ploog's theory (1985), as compared to other analytic approximations of the electron gas. Their assumption that higher subband electrons are located at the z-coordinate where the conduction band energy and the subband energy are equal (and the subsequent influence on conduction band profile) is an excellent substitute for the real case.

Figure 2 also compares the electron charge distributions in the channel, obtained through classical (Fermi statistics) and quantum simulations. It is easily noticed that the latter approach gives rise to a typically quantum electron distribution with local maxima corresponding to higher subbands. At liquid nitrogen temperature, the carrier profile in the channel tends to be sharp, with steep slopes on either side (see Fig. 3). At room temperature, the number of local maxima is higher leading to a wider distibution at lower electron concentrations (in bulk GaAs). A similar carrier profile (with local maxima) was measured by the C–V method in I^2-HEMTs (Kinoshita *et al.* 1986). To the author's knowledge, the only other theoretically estimated carrier profile in the channel was given by Yoshida (1986) and it does not reveal any local maxima. Although it leads to practically the same overall two-dimensional charge density in the channel, the Fermi-Dirac approach (Fig. 2) is seen to overestimate interface charge and to underestimate the center of mass of the electron distribution. The latter directly affects the value of the gate capacitance. The error becomes larger at lower temperatures.

As a general rule, the electron distribution in the channel is more scattered at low bias voltages and 2-DEG concentrations (Fig. 2) and gets thinner as the gate voltage and 2-DEG concentration increase (Fig. 3), while the subband spacings become larger.

4.2. *Behaviour of double- and multiple-heterojunction FETs*

As expected, the double-heterojunction device (Figs. 4 and 5) exhibits an enhancement of the electron concentration under similar bias conditions. The higher carrier concentration is caused by the increased donor charge, available in the left and right barrier layers, and hardly at all by the rectangular shape of the well, which lowers the first subband energy value and increases subband spacing. Remarkably, for the DH-device in Table 2, the subband separation $E_1 - E_0$ is pinned at 100 meV, even though the gate bias varies from -0.6 to $0{\cdot}3$ V. As a consequence, in the 100 Å-well DH-MODFET, more than 95% of the electron population resides on the lowest subband for a wide range of bias voltages. Since the lowest subband is closer to the conduction-band edge in the DH than in the SH device, mobilities should be higher in the first structure at room temperature. This phenomenon can be inhibited by the larger proportion of electrons that tunnel in the adjacent AlGaAs barrier layers and by the lower layer-quality of fabricated DH-FETs. Still, mobilities as high as $1{\cdot}2 \times 10^5\,\mathrm{cm^2/Vs}$ have been measured at 77 °K in a 100 Å-well transistor, confirming this judgement (Hikosaka *et al.* 1986).

The reduced bias and temperature dependence of the 2-DEG eigen-energies in the well is a consequence of the fact that the quantum well is defined by the band offset (less sensitive to temperature alterations and approximately insensitive to doping and bias if the channel is open). The situation departs from this ideal case if the quantum channel is wide or reverse biased (Figs. 4 and 5). In this device nearly 33% of the channel charge occupies the second subband and a third level has

Copyright © 2001. All Rights Reserved.

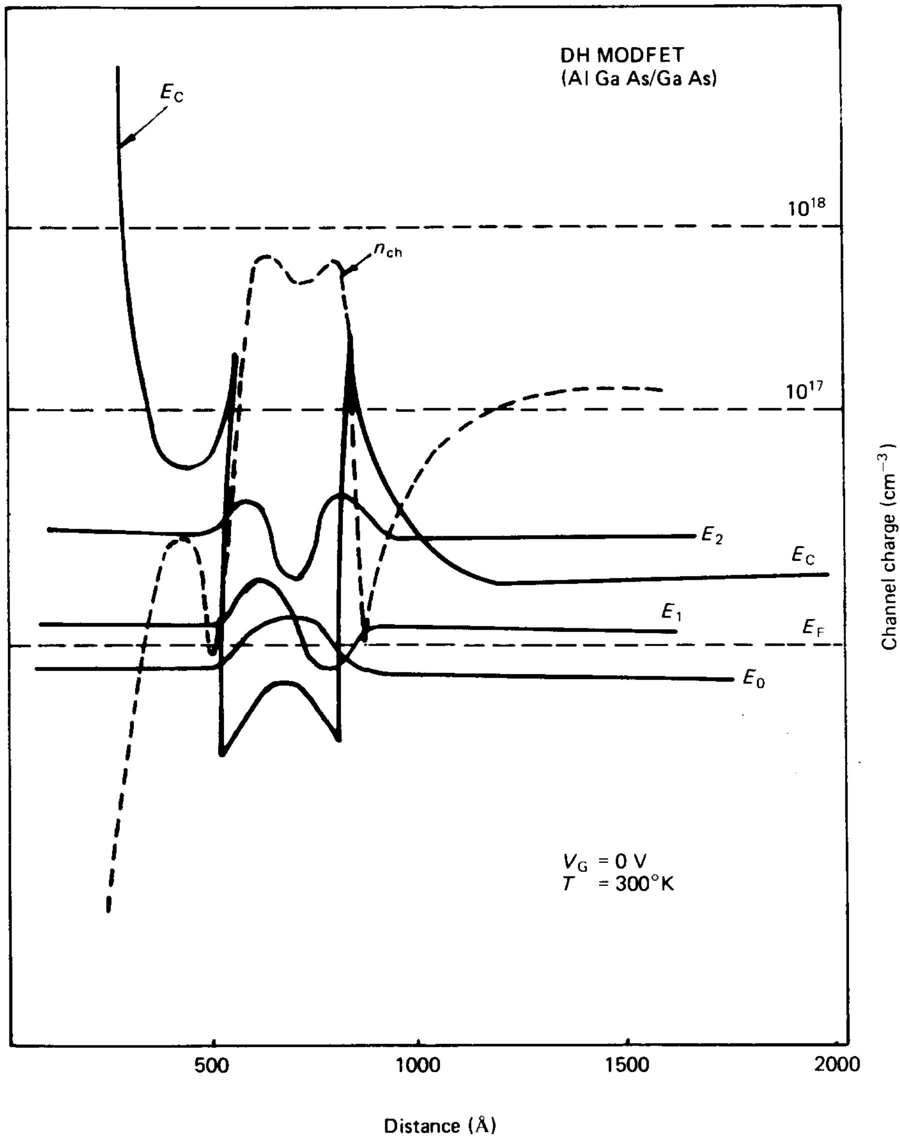

Figure 5. Electron profiles for the zero-biased DH-MODFET of Figure 4 at room temperature. Carriers in the barrier regions have also been plotted. The eigen-energies, relative to the minimum of the conduction band, are listed below:

$$E_0 = 0{\cdot}0447\,\text{eV};\quad Ns_0 = 7{\cdot}18\ 10^{11}\,\text{cm}^{-2};$$
$$E_1 = 0.0686\,\text{eV};\quad Ns_1 = 3{\cdot}81\ 10^{11}\,\text{cm}^{-2};$$
$$E_2 = 0{\cdot}1189\,\text{eV};\quad Ns_2 = 0{\cdot}70\ 10^{11}\,\text{cm}^{-2}.$$

emerged. Still, the overall charge is little changed because, as is the case with all simulated devices, SH-, DH- or MH-MODFETs, the sum total of the electron charge in the channel is set by the gate voltage and ionized donor concentration in the barrier layers, and not by band profiles. The latter adjust themselves, relative to the imref, according to the former. This explains why the average overall 2-DEG charge was little affected by the effective mass approximation, despite the altered

Copyright © 2001. All Rights Reserved.

distribution among subbands. Details of how this approximation influences the accuracy of SH- and DH-MODFET simulations will be addressed elsewhere. It is only mentioned here that the error can be as high as 8% with higher order subbands in wide channel DH devices.

The investigation of DH transistors can be used in the understanding of multiple channel (also known as multiple quantum well) devices (Saunier and Lee 1986). In these structures, a narrow barrier layer separating adjacent channels could lead to subband splitting due to the quantum coupling of the two wells. Figure 6 shows a schematic representation of this phenomenon. The analysis was performed analytically and numerically on an idealized band structure, neglecting the self-consistent influence of channel charge on conduction band profiles. In comparison with the 100 Å single-well structure, this structure exhibits two closely spaced (1 meV) lower subbands and two higher (more loosely spaced 6–7 meV) subbands. The energy spacing between these two sets of subbands is approximately equal to the subband separation in the single well. The coupling reduces (as does the splitting) with widening barrier layers. When the barrier layer becomes large enough, roughly more than 100 Å in this case, the two channels are completely de-coupled. In closely-spaced channel devices, as can be gathered from Figs. 5 and 6, a large proportion of elec-

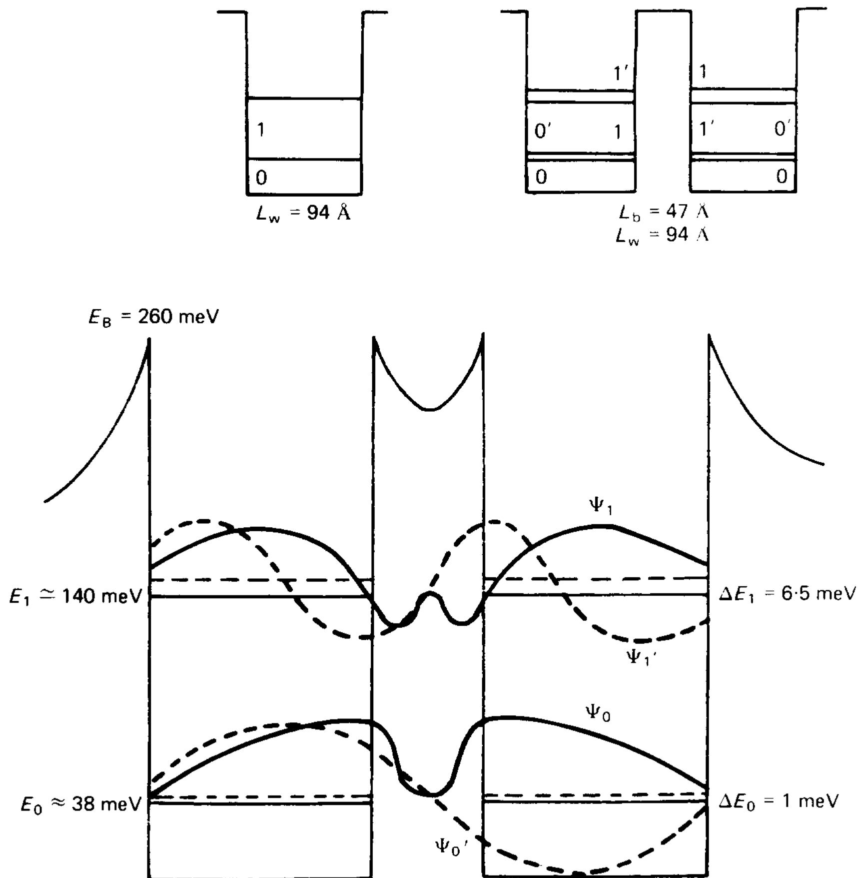

Figure 6. Subbands and wave functions in an idealized quadruple heterojunction structure with quantum channel coupling.

Copyright © 2001. All Rights Reserved.

trons are located in the low mobility/low velocity AlGaAs barrier, deteriorating transistor performance. Even with large barrier layers between adjacent channels, electron-wave-function coupling will remain a problem because of the emergence of a middle channel due to band bending. However, in narrow channels, this phenomenon will affect mainly the second and higher subbands, which often have a low occupancy and the effect on the overall electron concentration will be relatively small. From the wave-function profiles, it is clear that a two-channel MODFET would accommodate almost twice as many free carriers as does the single-channel device of similar well geometry (triangular or rectangular) leading to increased power capability. Compared to the corresponding SH device, the increase is not four-fold because quite a few carriers are wasted in the middle barrier layer (Figs. 5 and 6).

Despite these encouraging results, renewed efforts are required to clarify the minor, though systematic, conflict which appears between calculated and measured overall 2-DEG charge, in all investigated structures. This is a problem other investigators have not raised or chose to ignore, although examination of their main results confirms its presence in SH-MODFETs (Vinter 1984, Stern and Das Sarma 1984, Ponse *et al.* 1985). Irrespective of the theoretical approach (quantum or Fermi-Dirac, effective or energy-dependent mass), the computed electron concentration in the channel is higher at 77 °K than at 300 °K for identical bias conditions (contrary to existing experimental data which, however, are rather unclear about actual bias voltages). The constant Fermi level, assumed in the present model, is a reasonable and almost universally accepted approximation for MODFET structures operating up to moderate forward gate bias and cannot be seriously blamed for this anomaly, least of all at 0 V (Ponse *et al.* 1985). A study of the ionized donor charge, as described by eqn. (7), has indicated that, even with 100% deep traps ($s = 0$), the integral of the ionized donor charge over the AlGaAs layer is larger at 77 °K, while that of the total free charge (barrier and channel) is smaller than at 300 °K. It is highly probable that the measured 2-DEG charge includes the electrons in the AlGaAs region, thus explaining the aforementioned discrepancy. All investigated structures have revealed much lower electron concentrations in the barrier at 77 °K, compensation of the donor charge requiring more electrons in the channel.

5. Conclusion

The quantum model has been successfully used to derive the accurate electron-gas charge and wave-function profiles for various bias conditions in single and multiple heterojunction FETs.

Computer results are in good agreement with experimental data. In narrow-channel, forward-biased DH-MODFETs the analytic rectangular-well-approach compares favourably with quantum computer analyses. However, at reverse bias and devices with channels wider than 100 Å, the bottom of the conduction band in the well is strongly distorted from the rectangular one and the analytic solution yields poor results. Computations have revealed that the width of the rectangular channel hardly influences the overall 2-DEG charge if the doping profile in the device is not altered. Consequently, narrow channels should be preferred because most electrons will reside on the ground level at high velocities and subband spacing will be large. In MH-MODFETs this will also reduce quantum coupling of adjacent channels.

Copyright © 2001. All Rights Reserved.

In all studied cases, the electron distribution in the channel presents an absolute maximum (correlated with the wave-function maximum on the lowest subband) followed by decreasing local kinks corresponding to higher subbands. Such electron profiles have been measured in I^2-HEMTs but not noticed in self-consistent calculations performed by other authors. The local maxima are more pronounced in devices with fewer subbands (DH-MODFETs and SH-MODFETs at 77 °K). The quantum charge profile in the channel will directly reflect on the computed value of the gate capacitance. The classical Fermi-Dirac approach, which leads to reduced spreading of the electron profiles at the heterojunction interface in SH-MODFETs, will overestimte the capacitance. However, at 300 °K in SH-MODFETs, the error is acceptable.

Acknowledgments

The author is greatly indebted to Professor D. Dascalu for his constant support and encouragement and to Professor M. Bodea for suggesting the idea of a course in bandgap-engineering devices for graduate and post-graduate students that spurred earlier interest in MODFETs. Dr. A. Silard's pertinent advice regarding the manuscript is also acknowledged.

References

Chang, C.-Y., Liu, W. C., Jame, M. S., Wang, Y. H., Luryi, S., and Sze, S. M., 1986, Induced base transistor fabricated by molecular beam expitaxy. *Electron Device Letters.*, **7,** 497–500.

Heiblum, M., Nathan, M. I., and Eizenberg, E., 1985, Measuring barrier heights in GaAs-AlGaAs and metal-AlGaAs junctions by internal photoemission. 43rd Annual Device Research Conference.

Hikosaka, K., Hirachi, Y., and Abe, M., 1986, Microwave power double-heterojunction HEMTs. *I.E.E.E. Transactions on Electronic Devices*, **33,** 583–589.

Kawai, H., Kaneko, K., and Watanabe, N., 1984, Photoluminescence of AlGaAs/GaAs quantum wells grown by metalorganic chemical vapor deposition. *Journal of Applied Physics*, **56**(2), 463–467.

Kinoshita, H., Ishida, T., Inomata, H., Akiyama, M., and Kaminishi, K., 1986, Submicrometer insulated-gate inverted structure HEMT for high-speed large-logic-swing DCFL gate. *I.E.E.E. Transactions on Electronic Devices*, **33,** 608–615.

Laux, S. E., and Stern, F., 1986, Electron states in narrow gate-induced channels in Si. *Applied Physics Letters*, **49**(2), 91–93.

Lee, K., Schur, M. S., Drummond, T. J., and Morkoç, H., 1983, Electron density of the two-dimensional electron gas in modulation doped layers. *Journal of Applied Physics*, **54,** 2093–2095.

Matsumoto, K., Ogura, M., Wada, T., Yao, T., Hayashi, Y., Hashizume, N., Kato, M., Endo, T., Yamazaki, H., Inage, H., and Yamada, M., 1985, p-Channel GaAs SIS FET self-aligned by ion-implantation. 43rd Annual Device Research Conference.

Messiah, A., 1970, *Quantum Mechanics* (Amsterdam: North-Holland Publishing Company).

Morkoç, H., Bandy, S. G., Shankaran, R., Antypas, F. G. A., and Bell, R. L., 1978, A study of high-speed normally off and normally on $Al_{0.5}Ga_{0.5}As$ heterojunction gate FETs (HJFET). *I.E.E.E. Transactions on Electronic Devices*, **25,** 619–627.

Pierret, R. F., 1985, Extension of the approximate two-dimensional electron gas formulation. *I.E.E.E. Transactions on Electronic Devices*, **32,** 1279–1287.

Ponse, F., Masselink, W. T., and Morkoç, H., 1985, Quasi-Fermi level bending in MODFETs and its effect on FET transfer characteristics. *I.E.E.E. Transactions on Electronic Devices*, **32,** 1017–1023.

Copyright © 2001. All Rights Reserved.

POSPIESZALSKI, M. W., WEIREB, S., and CHAO, P.-C., MISHRA, U. K., PALMATEER, S. C., SMITH, P. M., and HWANG, J. C. M., 1986, Noise parameters and light sensitivity of low-noise high-electron-mobility transistors at 300 °K and 12·5 °K. *I.E.E.E. Transactions on Electronic Devices*, **33,** 218–223.

RAVAIOLI, U., and FERRY, D. K., 1986, MODFET ensemble Monte Carlo model including the quasi-two-dimensional electron gas. *I.E.E.E. Transactions on Electronic Devices*, **33, 677–681.**

SAUNIER, P., and LEE, J. W., 1986, High-efficiency millimeter-wave GaAs/GaAlAs power HEMTs. *Electron Device Letters*, **7,** 503–506.

SCHUBERT, E. F., and PLOOG, K., 1985, Electron subband structure in selectively doped n-AlGaAs/GaAs heterostructures. *I.E.E.E. Transactions on Electronic Devices*, **32,** 1868–1873.

STERN, F., and DAS SARMA, S., 1984, Electron energy levels in GaAs-$Ga_{1-x}Al_xAs$ heterojunctions. *Physics Review, B*, **30,** 840–845.

TAKAKUWA, H., TANAKA, K., MORI, Y., ARAI, M., KATO, Y., and WATANABE, S., 1986, A low-noise microwave HEMT using MOCVD. *I.E.E.E. Transactions on Electronic Devices*, **33,** 593–600.

THORNE, R. E., SU, L., FISCHER, R. G., KOPP, W. F., LYONS, W. G., MILLER, P. A., and MORKOÇ, H., 1983, Analysis of camel gate FETs (CAMFETs). *I.E.E.E. Transactions on Electronic Devices*, **30,** 212–216.

VINTER, B., 1984, Subbands and charge control in a two-dimensional electron gas field-effect transistor. *Applied Physics Letters*, **44,** 307–309.

WEILER, M. H., and AYASLI, Y., 1984, DC and microwave models for AlGaAs/GaAs high electron mobility transistors. *I.E.E.E. Transactions on Electronic Devices*, **31,** 1854–1890.

YOSHIDA, J., 1986, Classical versus quantim mechanical calculation of the electron distribution at n-AlGaAs/GaAs heterointerface. *I.E.E.E. Transactions on Electronic Devices*, **33,** 154–156.

Copyright © 2001. All Rights Reserved.